JOURNAL OF QUATERNARY SCIENCE (2016) **9999**(9999) 1–14 ISSN 0267-8179. DOI: 10.1002/jqs.2895

Optical dating of loessic hillslope sediments constrains timing of prehistoric rockfalls, Christchurch, New Zealand

Q1REZA SOHBATI,[1,2]* JOSH BORELLA,[3] ANDREW MURRAY,[2] MARK QUIGLEY[3,4] and JAN-PIETER BUYLAERT[1,2]
[1]Centre for Nuclear Technologies, Technical University of Denmark, DTU-Nutech, DTU Risø Campus, DK-4000, Roskilde, Denmark
[2]Nordic Laboratory for Luminescence Dating, Department of Geoscience, Aarhus University, DTU Risø Campus, DK-4000, Roskilde, Denmark
[3]Department of Geological Sciences, University of Canterbury, New Zealand
[4]School of Earth Sciences, The University of Melbourne, Victoria 3010, Australia

Received 1 February 2016; Revised 27 July 2016; Accepted 18 August 2016

ABSTRACT: Developing a robust chronology for mass-movement events is of crucial importance to understanding triggering mechanisms and assessing hazards. We constrain the emplacement time of four palaeorockfall boulders near Christchurch, New Zealand, using optically stimulated luminescence (OSL) of quartz and infrared stimulated luminescence dating (IRSL) of K-feldspar from loessic hillslope deposits underlying and upslope of individual boulders. The quartz OSL and K-feldspar $pIRIR_{290}$ ages are all consistent with the stratigraphy and in excellent agreement with each other, indicating that all the boulders that overlie the *in situ* loess must have been emplaced <13 ka ago. A comparison of luminescence ages with cosmogenic ^{3}He surface-exposure ages from the surfaces of each boulder shows that two out of four boulders contain pre-deposition ^{3}He inheritance. Overall, the optical ages are consistent with both a prehistoric rockfall event at 6–8 ka and a possible preceding event at 12–14 ka. This study is the first to show a successful application of luminescence dating to New Zealand colluvium loess and demonstrates the great advantage of a multi-technique approach in mass-movement dating.

Introduction

Mass movements such as rockfalls, landslides and debris flows pose a serious hazard to human population and infrastructure in mountainous areas. At least 300 million people are exposed to these events worldwide (Dilley *et al.*, 2005) and every year there are tens of reports of major mass movements around the world; these cause human fatalities (e.g. Bunce *et al.*, 1997; Guzzetti, 2000; Baillifard *et al.*, 2003; Massey *et al.*, 2014), destroy buildings (e.g. Evans and Hungr, 1993; Yin *et al.*, 2009) and damage transportation corridors (e.g. Hungr *et al.*, 1999; Budetta, 2004). Determining the return frequency of such events is central to understanding their driving mechanisms and estimating their hazard. Unfortunately, establishing this timing is notoriously difficult due to the lack of reliable geochronological tools. Different techniques have been developed with the object of providing a chronology for past rockfall activity (Lang *et al.*, 1999; Panek, 2015). These range from studying the degree of rock-surface weathering (e.g. Nesje *et al.*, 1994) to lichenometry (e.g. Bull *et al.*, 1994; Luckman and Fiske, 1995; André, 1997; McCarroll *et al.*, 2001), dendrochronology (e.g. Stoffel, 2006), radiocarbon (^{14}C) dating (e.g. Stout, 1969; Bertolini, 2007), optically stimulated luminescence (OSL) dating (e.g. Balescu *et al.*, 2007; Chapot *et al.*, 2012) and cosmogenic nuclide (CN) surface-exposure dating (e.g. Rinat *et al.*, 2014; Stock and Collins, 2014; Mackey and Quigley, 2014). All these techniques suffer from major uncertainties: most do not date the rockfall events directly and even CN dating cannot be easily applied because of problems resulting from inheritance of pre-event cosmogenic nuclides. Modern geochronology lays great emphasis on a multi-technique approach as this helps verify results from different techniques and reduce ambiguity in chronology. For example, using a novel approach of OSL dating directly applicable to rock surfaces, Chapot *et al.* (2012) determined the burial age of a fallen boulder as well as the underlying sediment in order to date a rockfall event that removed parts of a Barrier Canyon Style rock art in south-eastern Utah, USA. They supported the OSL ages by ^{14}C dating of a cottonwood leaf serendipitously found immediately between the boulder and underlying sediment (Chapot *et al.*, 2012). In another example, Matmon *et al.* (2005) determined the age of three different rockfall events along the margins of the Dead Sea fault using a combination of CN dating of the fallen boulders and OSL dating of underlying deposits.

Earthquakes are one of the major causal mechanisms for slope failure, and rockfalls are, in turn, the most abundant type of landslide induced by earthquakes (Keefer, 1984). In South Island, New Zealand, earthquake-induced rockfalls are frequently embedded in loessic sediments (Heron *et al.*, 2014); direct CN dating (Mackey and Quigley, 2014) and robust chronologies for loess accumulation and remobilization can thus be used to constrain the timing of these rockfalls. Luminescence is widely used to date loessic materials around the world (Roberts, ~~2012~~Q2, and references therein) but luminescence dating of loess from South Island is perceived to be challenging (e.g. Almond *et al.*, 2007). This perception is mostly based on studies using thermoluminescence (TL) and infrared stimulated luminescence (IRSL) of polymineral fine grain (i.e. 4–11 μm) fractions from loess deposits in Westland, Southland and Canterbury (Berger *et al.*, 2001a,b, 2002). The ages obtained have been reported to be anomalously young or old with low precision and in some cases in stratigraphically reversed sequence (Almond *et al.*, 2001, 2007). The undesirable luminescence characteristics have been attributed to the highly weathered nature of these sediments and the dominance of albites compared to

*Correspondence to: R. ~~Sohbati~~, [1]Centre for Nuclear Technologies, as above.
E-mail: resih@dtu.dk

K-rich feldspars (Berger *et al.*, 2001a; Almond *et al.*, 2001). With technical and instrumental developments in luminescence dating techniques, later studies have reported more reliable ages for loessic material from the South Island even though some age inconsistencies, mainly attributed to anomalous fading of IRSL signals from K-feldspars, still occurred (Litchfield and Lian, 2004; Preusser *et al.*, 2005). There have been few successful studies utilizing OSL dating of quartz (Holdaway *et al.*, 2002; Rowan *et al.*, 2012[Q3]; Hornblow *et al.*, 2014), probably due to reports on low OSL signal intensities and large changes in sensitivity (e.g. Preusser *et al.*, 2006); none of these attempted to date loess. We are unaware of any prior attempts to (i) use 'paired' quartz OSL and K-feldspar IRSL dating to rigorously test the reliability of luminescence ages from New Zealand sediments, (ii) apply luminescence dating to larger grain size (i.e. >11 μm) fractions of loess from the South Island, and (iii) apply luminescence dating to a steep, high-energy hillslope containing both *in situ* and colluvial (reworked) loessic sediments.

In this study, we use coarse-grained quartz OSL and K-rich feldspar IRSL signals to date loessic deposits south of Christchurch, New Zealand (Fig. 1a). We show that these techniques provide consistent and robust sediment chronologies and give confidence in the results even in such challenging depositional environments. These loess deposits host numerous palaeorockfall boulders that have previously been dated by cosmogenic ^{3}He (Mackey and Quigley, 2014), enabling cross-validation of our optical ages with independent age control. The new luminescence ages allow us to refine the timing of palaeorockfall emplacement in an area of high rockfall hazard (Massey *et al.*, 2014). This study and that of Borella *et al.* (2016a, b)[Q4] represent the first use of luminescence dating to refine palaeorockfall chronologies in New Zealand and one of the first to ~~apply this technique~~ globally (Matmon *et al.*, 2005; Chapot *et al.*, 2012).

Site description and geological context

The study site (Rapaki Study Site) is located in the Port Hills of southern Christchurch, near the village of Rapaki on Banks Peninsula (Fig. 1a,b). It is a steep (~20–25°) grassy slope (Fig. 1b) composed of *in situ* loess deposits, overlying large basaltic rockfall boulders, and loessic colluvium deposits that contain basaltic clasts. A large number of boulders (>650) were dislodged from the steep source cliff upslope of the Rapaki Study Site during moment magnitude 6.2 and 6.0 earthquakes in Christchurch in 2011 (Fig. 1b). The palaeorockfall boulders identified on the same slope (Fig. 1b,c) have the same morphology, lithology and similar spatial distribution as modern boulders and imply that similar earthquakes are likely to have been responsible for past rockfall activity (Mackey and Quigley, 2014; Borella *et al.*, 2016a, b).

The loessic colluvium deposits have been remobilized by hillslope erosion and deposited downslope (Fig. 1c). Stratigraphic boundaries between *in situ* and colluvial units (Fig. 1c) have been distinguished on the basis of textural, compositional and grain-size variations (Borella *et al.*, 2016a, b). A palaeosol has been identified at the top of the *in situ* loess and the top of the most recent colluvium contains an A-horizon (Borella *et al.*, 2016a, b). The planar hillslope is dissected by numerous rills and channels (Fig. 1b), originating primarily from collapsed tunnel gullies, and contains sedimentary wedges formed upslope of prehistoric boulders. More detailed geomorphic and stratigraphic data for the study site are available in Borella *et al.* (2016a, b).

The source of the loess has been attributed to the proximal floodplains of the Waimakariri River (Fig. 1a) (Griffiths, 1973[Q6]), which primarily transports weathered greywacke from the Southern Alps out into the Canterbury Basin (Villaseñor *et al.*, 2016). The basaltic source rock immediately upslope of the Rapaki Study Site is not a likely source because of the absence of quartz and low abundance of K-feldspar in the source rock.

Constraints on the timing of regional loess accumulation consist of previous radiocarbon dating, optical dating and tephrochronology at other study sites on Banks Peninsula (Fig. 1a) (Griffiths, 1973[Q7]; Almond *et al.*, 2007), and cosmogenic ^{3}He dating of palaeorockfall boulders overlying the *in situ* loess (Mackey and Quigley, 2014). *In situ* loess at the Rapaki Study Site has been correlated to the Birdlings Flat loess (Borella *et al.*, 2016a, b). Intercalated volcanic ash within the Birdling's Flat loess (Fig. 1a) has been attributed to the 25 360 ± 160 cal a BP Kawakawa Tephra (Vandergoes *et al.*, 2013). Humic acid from the uppermost identified palaeosol near the top of a section of correlative loessic units yielded a ^{14}C age of 17 450 ± 2070 cal a BP (Griffiths, 1973[Q8]). Almond *et al.* (2007) obtained a feldspar IRSL age of 17 300 ± 1000 years from near the top of the sequence. They interpreted feldspar IRSL ages to be underestimates, and suggested loess accumulation initiated before ca. 30 000 ^{14}C a BP (ca. 35 000 cal a BP). Mackey and Quigley (2014) used cosmogenic ^{3}He surface-exposure dating to determine the emplacement time of 19 prehistoric rockfall boulders overlying the *in situ* loess. The apparent surface-exposure ages ranged from 6 to 70 ka with most ages between 6 and 20 ka; age concentrations at 6–8 and 12–14 ka were interpreted to reflect surface-exposure ages and older ages were attributed to pre-depositional inheritance (Fig. 1d). Borella *et al.* (2016a, b) obtained ^{14}C dates from charcoal within the uppermost layers of the reworked colluvial loess of ~1660–1880 AD (2σ). The *in situ* loess at the Rapaki Study Site is thus conservatively attributed to deposition beginning before ~30 ka and ending before 6–13 ka, while most of reworked colluvial loess is attributed to deposition after 6–13 ka and before 1660–1880 AD.

Methodology

Sampling, laboratory preparation and analytical facilities

Sampling for optical dating was targeted at five palaeorockfall boulders: three with credible exposure ages of <13 ka in stratigraphic order with the expected post-Last Glacial Maximum (LGM) depositional age of 17–13 ka for the underlying loess and two with exposure ages of >20 ka. Thirteen OSL samples were collected by hammering metal tubes (5 cm diameter and 15 cm length) into freshly cleaned trench walls: (i) eight samples from loess underlying the boulders, and (ii) five samples from reworked loess colluvium that accumulated behind the boulders after their emplacement on the hillslope (Fig. 1c,e). The samples underlying the boulders should predate their emplacement and thus give a maximum boulder emplacement age, whereas the accumulated deposits upslope of the boulders should post-date their deposition and so provide a minimum boulder emplacement age (Fig. 1e); by dating these samples we should be able to constrain the time window during which each boulder must have been put in place and thus determine the age of the responsible rockfall event.

Sediment was removed from sampling tubes under low-level orange light and potentially light-exposed material from the outer ends of the tubes was discarded; sediment from the middle of the tubes was then wet sieved to 40–63 μm. The

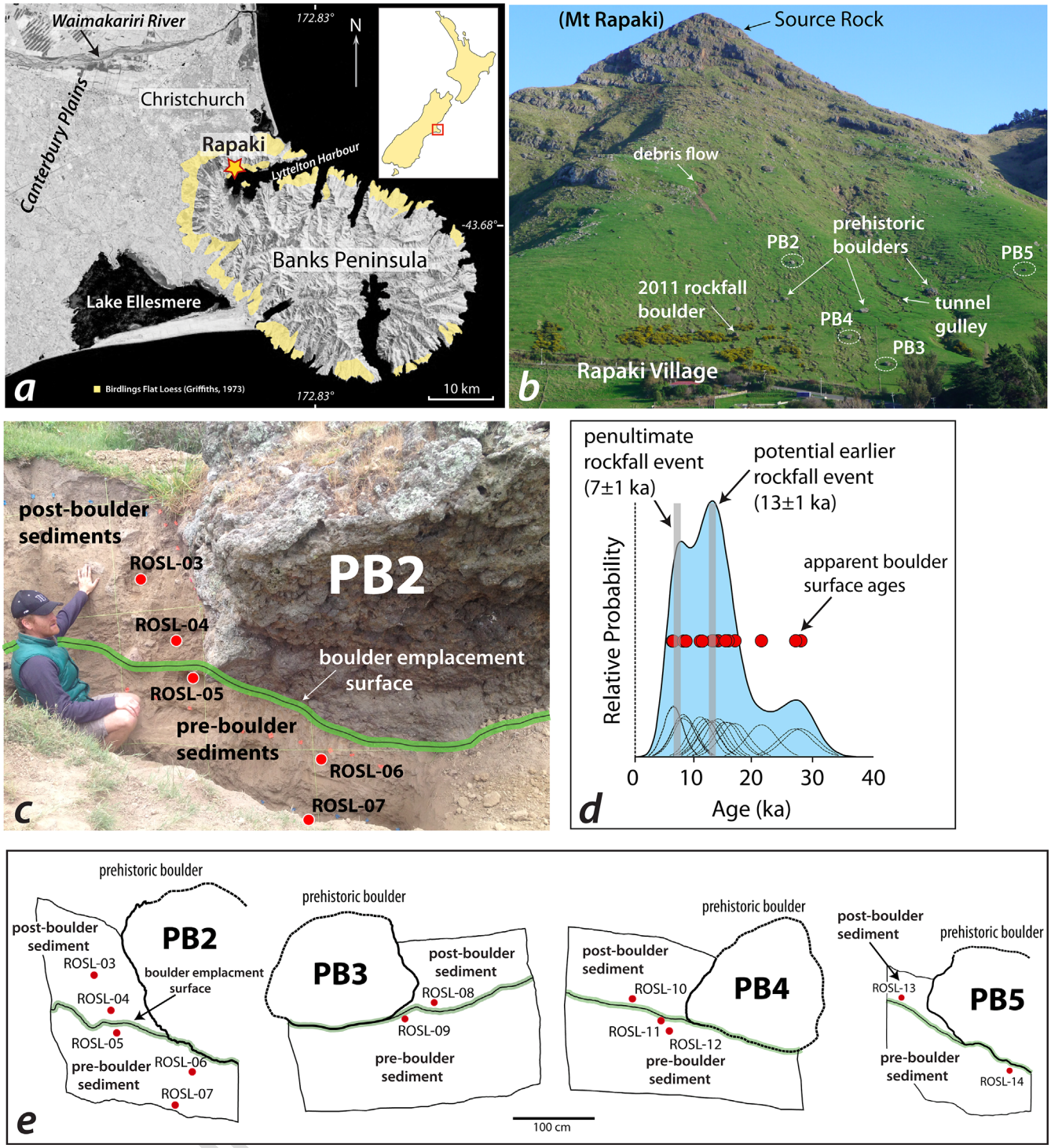

Figure 1. (a) Location of the study site, South Island, New Zealand. Distribution of Birdlings Flat Loess formation shown per Griffiths (1973)[Q5]. (b) A west-looking view of the slopes above Rapaki village showing the location of the studied palaeorockfall boulders. (c) A photo of one of the boulders (PB2) together with the location of the loess samples collected from colluvium deposits underlying and upslope the boulder. (d) Apparent ^{3}He surface-exposure ages of individual boulders indicated as Gaussian probability distribution functions (modified after Mackey and Quigley, 2014). (e) Schematic view of all the studied boulders with the location of the related luminescence samples. [Q5]

grains were treated with 10% HCl to remove carbonates and 10% H_2O_2 to dissolve any reactive organic material. They were then etched with 10% HF for 40 min to remove any alpha-irradiated surface layer and weathering products and coatings, followed by 10% HCl for 20 min to remove any fluoride contamination. The K-rich feldspar fractions were then separated in a water-based heavy liquid solution ($\rho = 2.58\,g\,cm^{-3}$; Fastfloat). The quartz grains were further treated with hydrofluorosilicic acid for 2 weeks, followed by 10% HCl.

All luminescence measurements were carried out using a Risø TL/OSL reader (model TL-DA 20), with blue light stimulation ($\lambda = 470$ nm, $\sim 80\,mW\,cm^{-2}$) and photon detection through a 7.5-mm Hoya U-340 glass filter for quartz, and infrared stimulation ($\lambda = 875$ nm, $\sim 135\,mW\,cm^{-2}$) and photon detection through a Schott BG39/BG3 filter combination (2 and 3 mm, respectively) for K-feldspar (Bøtter-Jensen *et al.*, 2010[Q9]). Beta irradiations used a $^{90}Sr/^{90}Y$ source mounted on the reader and calibrated for both discs and cups using 180–250-μm calibration quartz grains (Hansen *et al.*, 2015). Grains were mounted [Q9]

as large (~9 mm diameter for quartz) or medium (~4 mm diameter for feldspar) aliquots in a monolayer using silicone oil on 9-mm-diameter stainless steel discs (quartz) or cups (feldspar). The heating rate was 5 °C s^{-1} throughout. All thermal treatments and stimulations at temperatures higher than 200 °C were carried out in nitrogen atmosphere, and a pause of 5 s was inserted before stimulation to allow all grains to reach the measurement temperature. Five empty channels were inserted before and after the stimulation to monitor any isothermal TL signals.

Dosimetry

Radionuclide concentrations (^{238}U, ^{226}Ra, ^{232}Th and ^{40}K) were measured using high-resolution gamma spectrometry on sediment collected from around the OSL sample tube. Approximately 50 g of sediment was dried at 50 °C, pulverized and homogenized, and then heated to 450 °C for 24 h to remove any organic matter. The material was then cast in wax to prevent radon loss and to provide a reproducible counting geometry. Samples were stored for at least 3 weeks to allow ^{222}Rn to reach equilibrium with its parent ^{226}Ra before being measured on a high-purity germanium detector for at least 24 h. Details of the gamma spectrometry calibration are given in Murray *et al.* (1987)[Q10]. The internal beta dose rate activity from ^{40}K was calculated based on an assumed effective potassium content of 12.5 ± 0.5% (Huntley and Baril, 1997), and the beta contribution from ^{87}Rb was calculated assuming a ^{87}Rb content of 400 ± 100 p.p.m. (Huntley and Hancock, 2001). For K-feldspar, a small internal alpha contribution of 0.10 ± 0.05 Gy ka^{-1} from internal ^{238}U and ^{232}Th was assumed and included in the dose rates, based on ^{238}U and ^{232}Th concentration measurements by Mejdahl (1987). For quartz, an internal dose rate of 0.010 ± 0.002 Gy ka^{-1} was assumed (Vandenberghe *et al.*, 2008). The radionuclide concentrations were converted to dose rate data using the conversion factors from Guérin *et al.* (2011). The contribution from cosmic radiation to the dose rate was calculated following Prescott and Hutton (1994)[Q11], assuming an uncertainty of 5%. The long-term water content (expressed as a percentage of dry weight) was assumed to be similar to the modern water content. Water content, radionuclide concentrations and dry, infinite-matrix beta and gamma dose rates are summarized in Table 1.

Results: luminescence characteristics and ages

Quartz

Quartz is the most widely used dosimeter in luminescence dating and the reliability of the quartz OSL single-aliquot regenerative-dose (SAR) protocol (Murray and Wintle, 2000) for dose determination is well established (e.g. Murray and Olley, 2002[Q12]). All the OSL measurements were performed at 125 °C for 40 s. A high-temperature blue-light stimulation at 280 °C was also carried out for 40 s at the end of each cycle to minimize the residual signal transfer between different cycles (Murray and Wintle, 2003) (Supporting Information, Table S1). Signal intensities were calculated using the initial 0.32 s of the signal, less an immediate background derived from the following 0.8 s. An early background subtraction was selected to minimize the contribution of the more difficult to bleach and more thermally unstable medium and slow components to the net signal (Jain *et al.*, 2003; Li and Li, 2006; Cunningham and Wallinga, 2010).

For all samples, the purity of quartz extracts was examined by measuring the OSL signal from three aliquots from each sample with and without prior infrared stimulation at room temperature for 100 s. The ratio of the two OSL signals, the so-called OSL infrared (IR) depletion ratio, was then calculated for each aliquot (Duller *et al.*, 2003[Q13]). The resulting average OSL IR depletion ratio was 0.974 ± 0.012 (n = 39), implying that any feldspar contamination of our quartz luminescence signals is negligible. Quartz extracts from all the samples were sensitive and the OSL signal was dominated by the fast component (Fig. 2).

The performance of our quartz OSL SAR protocol was verified using both natural and dose-recovery preheat-plateau tests. The natural preheat-plateau test was carried out to investigate the dependence of equivalent dose (D_e) on preheat temperature. Twenty-four aliquots of quartz from one of the samples were sorted into groups of three. Each of the eight groups was then treated with a different preheat temperature (between 160 and 300 °C for 10 s, with temperature increasing in 20 °C steps). The temperature of the second preheat treatment (that following the test dose, the so-called cut-heat temperature) was chosen to be 20 °C lower than that of the first preheat treatment. From Fig. 3(a) it can be seen that there is no systematic dependence of D_e on preheat temperature between 160 and 300 °C.

For the dose-recovery preheat-plateau test, 24 fresh aliquots were stimulated twice at room temperature for 100 s [Q10] using blue LEDs to fully reset the natural OSL signals. A pause of 1 ks was inserted between the two stimulations to allow for any charge trapped in shallow refuge traps (especially that associated with the 110 °C TL peak) to decay and subsequently partly refill the OSL trap before the second stimulation. The aliquots were then given a dose of ~36 Gy and measured in a similar manner as in the natural preheat-plateau test. Figure 3(b) summarizes the measured-to-given dose ratios at different preheat temperatures. It appears that the dose recovery ratio is poor for low preheat temperatures (<240 °C) but is satisfactory (within 10% of unity) for the 240–280 °C interval. The closest ratio to unity is 0.98 ± 0.06 (n = 3) at 260 °C, showing that a known laboratory dose [Q11] absorbed before any thermal pretreatment can be accurately measured at this preheat temperature. Accordingly, a preheat temperature of 260 °C (for 10 s) and a cut-heat temperature of 240 °C (for 0 s) were selected for all quartz OSL D_e measurements. A summary of the D_e values and calculated ages is given in Table 1.

K-rich feldspar

K-feldspar is an alternative dosimeter in luminescence dating. However, its application has been hampered because K-feldspar IRSL signals are usually not stable with time (e.g. Spooner, 1994; Huntley and Lamothe, 2001; Wallinga *et al.*, 2007). It is now broadly accepted that this athermal loss of signal, commonly called 'anomalous fading', is due to the [Q12] tunnelling of electrons from thermally stable traps to nearby recombination centres (Jain *et al.*, 2015). The presence of anomalous fading results in age underestimations (Aitken, 1985), but the use of K-feldspar as a dosimeter in luminescence dating has been increasing rapidly over the last few years since the recognition of the more stable IR signals measured after a low-temperature IR stimulation, the so-called post-IR IRSL signals (pIRIR) (Thomsen *et al.*, 2008; Buylaert *et al.*, 2009). We used a $pIRIR_{290}$ SAR protocol to measure the K-feldspar fractions from all the samples (Thiel *et al.*, 2011). A preheat treatment of 320 °C was applied for 60 s after natural, regenerative and test doses. The first IR stimulation at 50 °C (IR_{50}) was followed by a second IR stimulation at 290 °C ($pIRIR_{290}$). A high-temperature

Table 1. Summary of sample code, burial depth, radionuclide concentrations, ~~measured~~ water content, quartz OSL and K-feldspar IR_{50} and $pIRIR_{290}$ equivalent doses and ages. Residual doses of 1.2 and 6 Gy were subtracted from the IR_{50} and $pIRIR_{290}$ D_e values, respectively. Feldspar dose rates assume a K concentration of 12.5 ± 0.5% for K-feldspar (Huntley and Baril, 1997). An absolute error of 4% is assumed on the water content values.

Sample code	Sample name	Depth (cm)	Water content (%)	^{226}Ra ($Bq\,kg^{-1}$) ± se	^{232}Th ($Bq\,kg^{-1}$) ± se	^{40}K ($Bq\,kg^{-1}$) ± se	Total dose rate(Gy ka^{-1}) ± se	Quartz OSL D_e (Gy) ± se	*n*	Quartz OSL age (ka) ± se	K-feldspar IR_{50} D_e (Gy) ± se	K-feldspar $pIRIR_{290}$ D_e (Gy) ± se	*n*	K-feldspar $pIRIR_{290}$ age (ka) ± se
146601	ROSL-02 (PB1)	247	10	30.14 ± 1.08	40.07 ± 1.16	502 ± 16	2.65 ± 0.13	78 ± 5	17	29.3 ± 2.5	44.24 ± 1.14	84.3 ± 1.8	12	28.5 ± 1.6
146602	ROSL-08 (PB3)	81	14	35.8 ± 0.9	42.3 ± 0.9	554 ± 16	2.85 ± 0.12	8.14 ± 0.66	18	2.9 ± 0.3	4.07 ± 0.30	8.4 ± 0.4	12	2.6 ± 0.2
146603	ROSL-09 (PB3)	170	6	33.38 ± 1.14	38.5 ± 1.2	446 ± 16	2.76 ± 0.14	15.9 ± 1.2	18	5.8 ± 0.5	11.8 ± 0.6	19.9 ± 0.6	12	6.5 ± 0.4
146604	ROSL-10 (PB4)	93	11	32.7 ± 0.9	41 ± 1	473 ± 12	2.66 ± 0.12	11.0 ± 0.9	18	4.2 ± 0.4	7.4 ± 0.5	11.4 ± 0.5	12	3.8 ± 0.2
146605	ROSL-11 (PB4)	120	8	38.6 ± 1.9	42 ± 2	440 ± 30	2.55 ± 0.15	26 ± 2	18	10.25 ± 1.07	16.5 ± 0.5	29.8 ± 1.0	12	10.4 ± 0.7
146606	ROSL-12 (PB4)	131	7	33.8 ± 1.6	42.5 ± 1.7	510 ± 20	2.87 ± 0.16	38 ± 3	18	13.4 ± 1.2	23.7 ± 0.6	40.4 ± 0.6	12	12.7 ± 0.7
146607	ROSL-13 (PB5)	31	4	36.2 ± 1.7	42.8 ± 1.8	520 ± 20	3.18 ± 0.17	5.5 ± 0.4	22	1.7 ± 0.2	3.8 ± 0.3	6.8 ± 0.3	12	1.94 ± 0.14
146608	ROSL-14 (PB5)	110	8	35.9 ± 1.7	43.5 ± 1.9	460 ± 30	2.94 ± 0.16	30.0 ± 1.7	24	10.2 ± 0.8	22.7 ± 0.7	40.7 ± 0.9	12	12.6 ± 0.8
146609	ROSL-03 (PB2)	70	12	32.6 ± 1.2	39.877 ± 1.114	470 ± 20	2.69 ± 0.13	7.6 ± 0.7	24	2.8 ± 0.3	4.5 ± 0.3	7.4 ± 0.3	12	2.46 ± 0.15
146610	ROSL-06 (PB2)	87	7	31.9 ± 1.5	43.2 ± 1.4	490 ± 30	2.89 ± 0.15	35 ± 4	24	12.0 ± 1.4	18.5 ± 0.4	32.7 ± 0.7	12	10.2 ± 0.6
146611	ROSL-07 (PB2)	171	4	31.5 ± 1.6	49 ± 1.8	440 ± 20	2.93 ± 0.16	80 ± 8	22	27.2 ± 3.0	39.2 ± 1.4	70.5 ± 1.9	12	21.8 ± 1.4
146612	ROSL-04 (PB2)	99	12	35.8 ± 1.5	40.3 ± 1.4	460 ± 20	2.47 ± 0.13	19.0 ± 1.5	23	7.7 ± 0.8	11.13 ± 0.35	19.2 ± 0.3	12	6.9 ± 0.4
146613	ROSL-05 (PB2)	116	9	34.6 ± 1.6	40.4 ± 1.7	480 ± 20	2.79 ± 0.15	35 ± 2	17	12.47 ± 1.06	19.0 ± 0.3	33.7 ± 0.4	12	10.8 ± 0.6

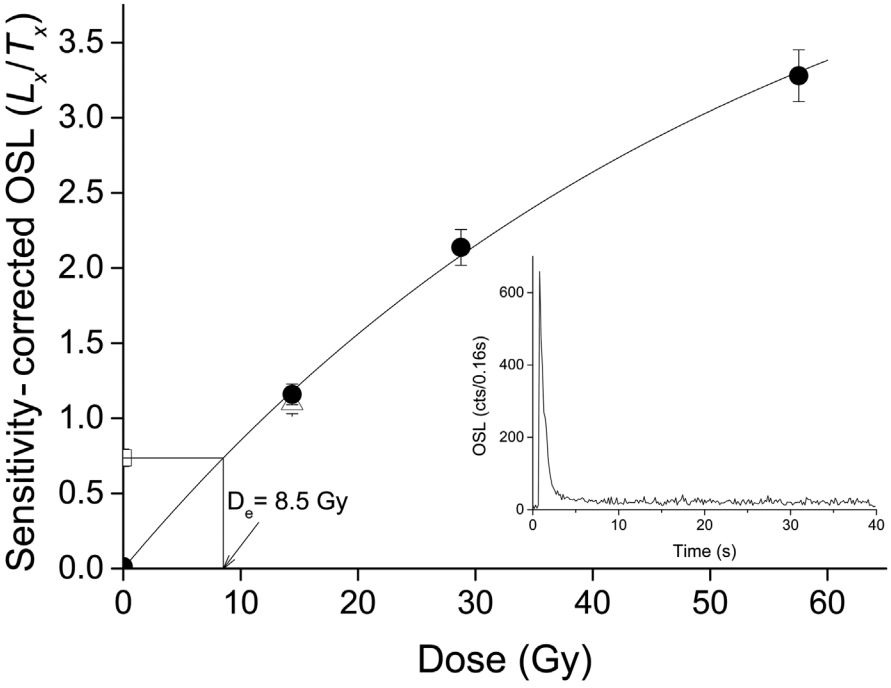

Figure 2. Quartz OSL dose–response curve. The inset shows the natural OSL decay curve for the same aliquot.

stimulation at 325 °C was also performed at the end of each SAR cycle to minimize signal carry-over to the next cycle. All IR stimulations were carried out for 100 s (Table S1). The signal derived from the first second of stimulation less a background from the last 10 s was used for all calculations.

To verify the reliability of the measurement protocol, a dose-recovery test was carried out by adding different known laboratory doses to the natural dose of the youngest sample. The largest added dose was selected in a way so the total dose is close to the $pIRIR_{290}$ D_e of the oldest sample. As can be seen from Fig. 4, while the IR_{50} dose recovery ratio is poor (~0.8), the $pIRIR_{290}$ dose recovery is satisfactory (within 10% of unity) over the entire dose range in our samples (Fig. 4). Similar low dose recovery ratios have been observed for the IR_{50} signal measured as a part of the $pIRIR_{290}$ protocol (e.g. Buylaert *et al.*, 2012; Schatz *et al.*, 2012; Tsukamoto *et al.*, 2013; Murray *et al.*, 2014). It has been argued that this may be due to a trapping sensitivity change caused by the

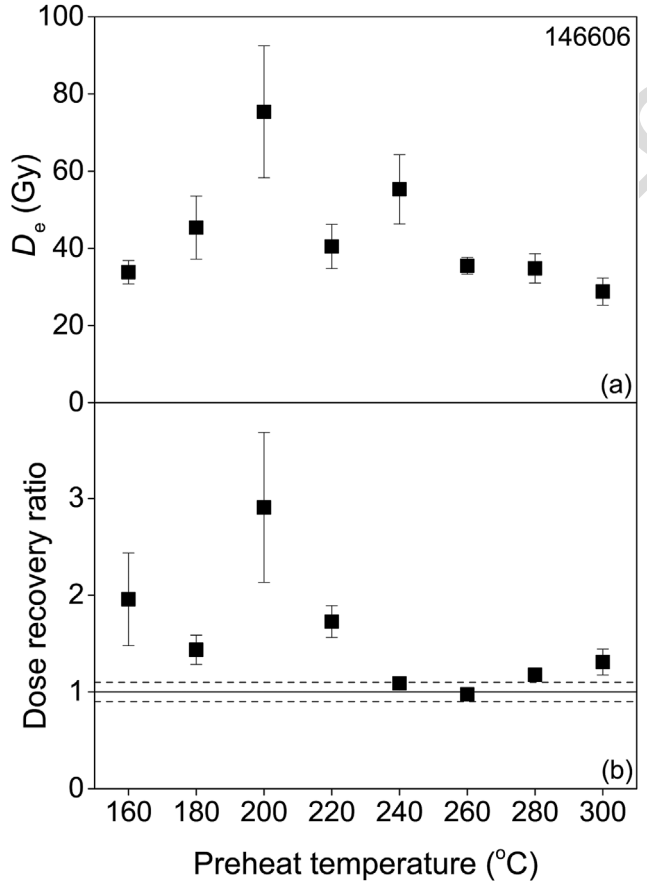

Figure 3. Results of (a) preheat-plateau and (b) dose–recovery preheat-plateau tests. Each data point is an average of three aliquots. The error bars represent one standard error.

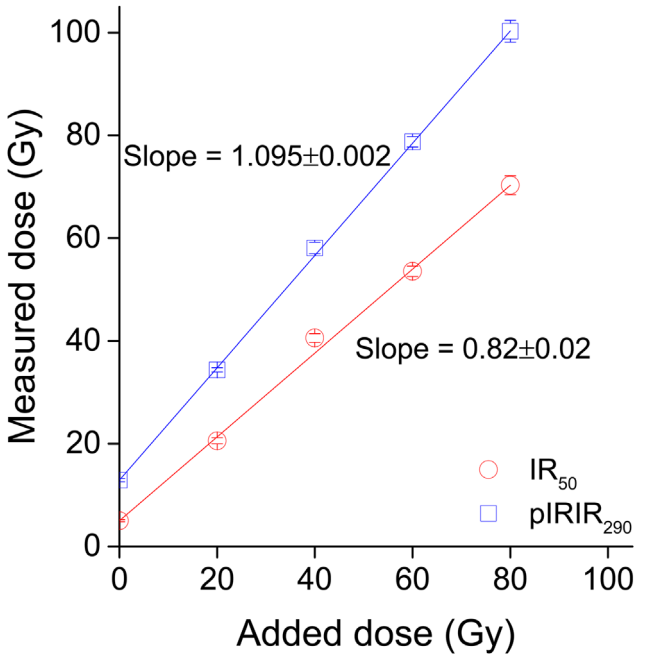

Figure 4. K-feldspar dose recovery test results. Each data point represents an average of three aliquots. The error bars show one standard error.

stringent preheating (here 320 °C for 60 s) of the sample before measuring the natural IR_{50} signal (Wallinga *et al.*, 2000). Kars *et al.* (2014a) show that this sensitivity change cannot be detected through test dose responses in the SAR protocol, and thus may result in an invalid equivalent dose estimation. We therefore do not use the IR_{50} equivalent doses for age calculation. ~~Instead~~, we ~~only~~ use these values in the discussion of incomplete bleaching.

Anomalous fading

To measure the stability of the IRSL signals in our samples, an anomalous fading test was carried out on the same aliquots as used for D_e determination. Anomalous fading is usually quantified by the 'g'-value, which is the fractional loss of signal during a storage period of one decade, where the storage periods are expressed as decades relative to the laboratory irradiation time (Aitken, 1985, *appendix* F). Three aliquots from each sample were measured to evaluate the 'g'-value using SAR cycles (Table S1), following Auclair *et al.* (2003). Each aliquot was given a regenerative dose close to the sample-averaged $pIRIR_{290}$ equivalent dose and a test dose equal to 50% of the regenerative dose was used. The ratios of regenerated signals (L_x) to test dose signals (T_x) were measured repeatedly, with time delays of ~0.22 h (IR_{50}) and ~0.27 h ($pIRIR_{290}$) for prompt measurements, and 12 h for delay measurements. The 'g'-values were calculated using eqn (4) of Huntley and Lamothe (2001) and normalized to a measurement delay time (t_c) of 2 days after irradiation (Fig. 5).

Fading rates showed no trends with depth or depositional environment [i.e. loess/(reworked) colluvium loess]. We therefore combined data of all the samples and obtained mean g_{2days} values of 0.7 ± 0.8 and 0.9 ± 0.3% per decade ($n = 39$) for the IR_{50} and $pIRIR_{290}$ signals, respectively. Several studies have documented similar fading rates of ~1% per decade for the $pIRIR_{290}$ signal, while the IR_{50} signal usually shows higher laboratory fading rates (e.g. Stevens *et al.*, 2011; Roberts, 2012; Roskosch *et al.*, 2012; Schatz *et al.*, 2012; Tsukamoto *et al.*, 2013). It has been suggested that such low fading rates (i.e. <1.5% per decade) are most likely an artefact of the measurement procedure and do not accurately reflect the signal instability in nature (e.g. Thiel *et al.*, 2011; Buylaert *et al.*, 2012; Roberts, 2012). The feldspar ages were not corrected for apparent laboratory fading.

Residual dose

Post-IR IRSL signals are known to be difficult to bleach as there remains a residual dose even after prolonged exposure periods in daylight or a solar simulator (e.g. Buylaert *et al.*, 2011; Lowick *et al.*, 2012; Reimann and Tsukamoto, 2012; Roberts, 2012; Li *et al.*, 2013; Kars *et al.*, 2014b). To determine the size of this residual dose in our samples we followed two different approaches. In the first method, 24 aliquots from the youngest sample were bleached in groups of three for different lengths of time (from 1 to 512 h, increasing by powers of 2) using an artificial daylight spectrum (Hönle SOL2 solar simulator) approximately six times more intense than full sunlight. The IR_{50} and $pIRIR_{290}$ residual doses were then measured in the usual manner (Table S1). For both signals the residual doses decrease slowly with bleaching time and appear to reach a constant after 64 h of bleaching (Fig. 6). The average IR_{50} and $pIRIR_{290}$ residual doses after an exposure time of 64 h are 1.24 ± 0.14 Gy ($n = 6$) and 6.15 ± 0.10 Gy ($n = 6$), respectively.

Sohbati *et al.* (2012) reported a correlation between the IR_{50} and $pIRIR_{225}$ equivalent doses and their corresponding residual doses (after laboratory bleaching) with finite intercepts on the residual dose axes. They interpreted these intercepts as unbleachable residual doses that would have been present in their samples, had they been fully bleached at the time of deposition. Similar observations have been made by various workers for different pIRIR signals (e.g. Buylaert *et al.*, 2012; Schatz *et al.*, 2012; Sohbati *et al.*, 2013; Tsukamoto *et al.*, 2013; Veit *et al.*, 2015; Qiu and Zhou, 2015[Q14]). In the second method, we followed a similar approach; three aliquots per sample were first bleached for 4 h in a Hönle SOL2 solar simulator. The IR_{50} and $pIRIR_{225}$ residual doses were then measured and plotted against the corresponding D_e values for each sample. As Fig. 7 shows,

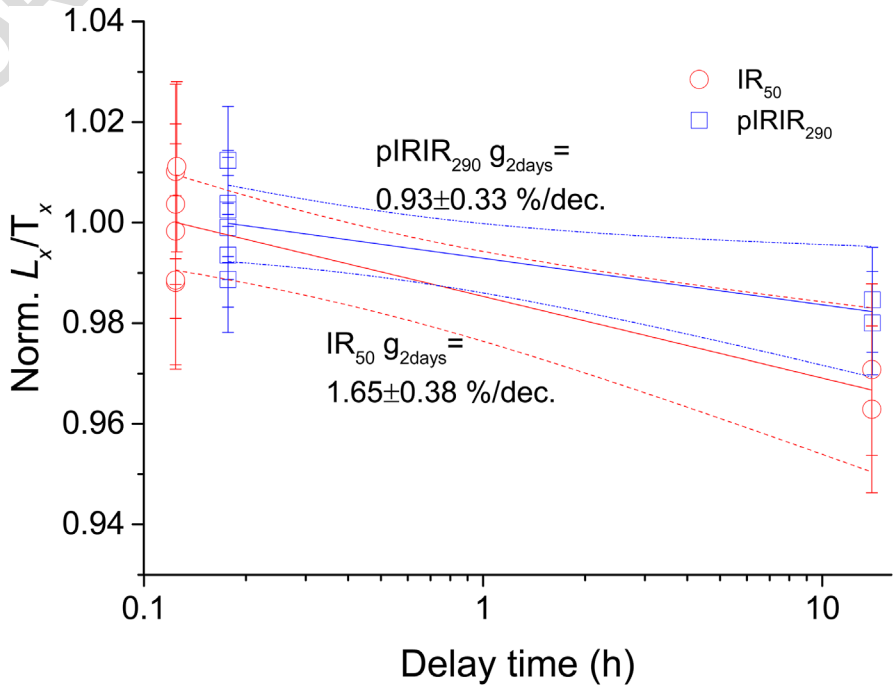

Figure 5. Example of a g-value measurement on a single aliquot of sample 146611.

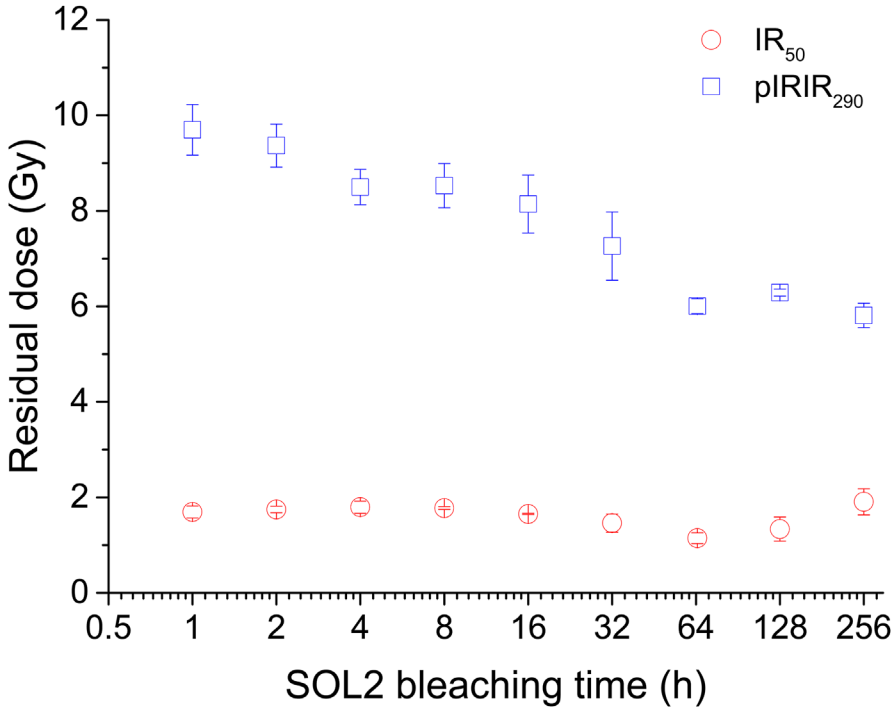

Figure 6. IR_{50} and $pIRIR_{290}$ residual doses in sample 146607 plotted against exposure time in a Hönle SOL2 solar simulator. Each data point is an average of three aliquots and error bars represent one standard error.

there is a clear correlation between the residual doses and the equivalent doses. The intercepts of the linear fits to the IR_{50} and $pIRIR_{290}$ data are 1.6 ± 0.3 and 5.9 ± 0.5 Gy, respectively. Interestingly, these values are comparable to the residual doses observed in the youngest sample after 64 h of bleaching, and are similar to the values reported in the literature for the same signals (e.g. Buylaert *et al.*, 2012; Schatz *et al.*, 2012; Kars *et al.*, 2014b; Murray *et al.*, 2014; Yi *et al.*, 2015). It is not clear whether these residual doses originate from a truly unbleachable IRSL component or arise from the transfer of charge from light-insensitive traps to IR-sensitive trap(s) during preheating, so-called thermal transfer (e.g. Aitken, 1998; Buylaert *et al.*, 2011). In either case, they would correspond to residual doses present in a fully bleached, modern sample and are likely to have been present in all our samples at the time of deposition. The resulting IR_{50} and $pIRIR_{290}$ D_e values after residual dose subtraction and the calculated $pIRIR_{290}$ ages are given in Table 1.

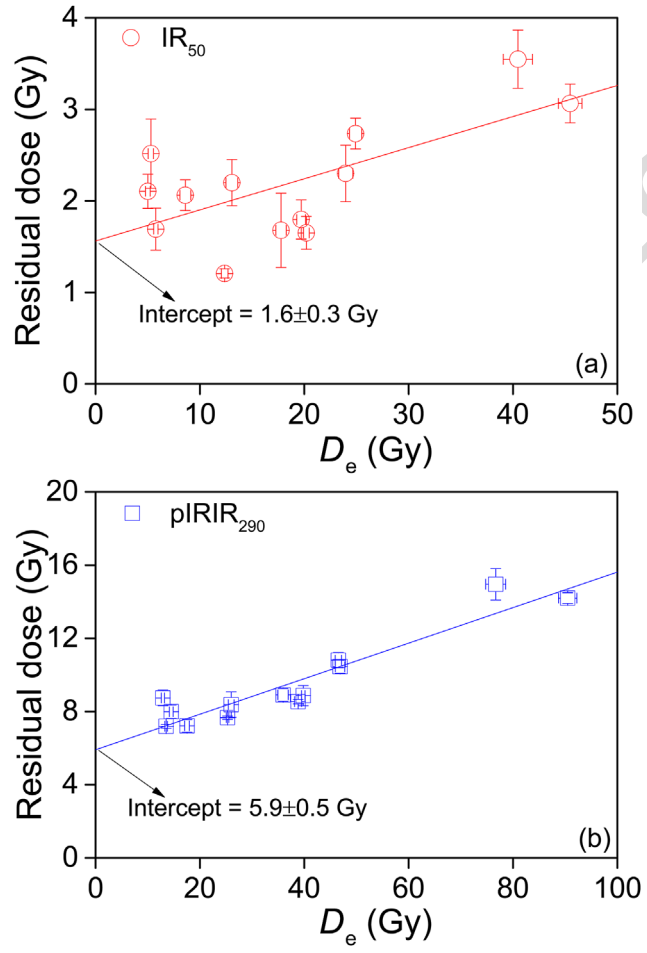

Figure 7. (a) IR_{50} and (b) $pIRIR_{290}$ residual doses versus their corresponding D_e values for all the samples. The solid lines represent the best linear fits to the data.

Discussion

Reliability of the luminescence ages: were the samples well bleached?

The laboratory behaviour of the quartz OSL signals from these samples of New Zealand loess is satisfactory and the dose recovery for the sample tested under the chosen measurement conditions is consistent with unity (0.98 ± 0.06; $n = 3$). Thus, for these samples it appears that our measurement protocol is appropriate for the measurement of dose. As discussed in the Introduction, this is in contrast to earlier work on quartz from South Island. With the exception of a few studies (Holdaway *et al.*, 2002; Rowan *et al.*, 2012[Q15]; Hornblow *et al.*, 2014), previous luminescence dating investigations have concluded that quartz was insensitive and unsuitable for dating (e.g. Preusser *et al.*, 2006; Almond *et al.*, 2007). Q15

Similarly, our feldspar IRSL dosimetry signal is also well behaved. The slope of the measured to given dose relationship for the $pIRIR_{290}$ signal is within 10% of unity, and laboratory fading rates are not considered significant [g_{2days} values of 0.7 ± 0.8 and 0.9 ± 0.3% per decade ($n = 39$) for the IR_{50} and $pIRIR_{290}$ signals, respectively]. Previous work suggested that ages based on ambient temperature feldspar IRSL signals underestimated independent age control (presumably due to anomalous fading) and this was blamed on the apparently high degree of weathering (Almond *et al.*, 2001).

A major challenge in luminescence dating of hillslope deposits is incomplete bleaching (Fuchs and Lang, 2009). The colluvial deposits accumulated behind the boulders were reworked by slope processes and thus, because of short transport distances and mixing during transportation, may not have been well bleached. Fuchs and Lang (2009) also point out that one way to identify insufficient bleaching may be to use luminescence signals of different bleaching characteristics. Several studies have shown that the quartz OSL signal resets faster than the K-feldspar IR_{50} signal and that the IR_{50} signal, in turn, bleaches more rapidly than the elevated temperature pIRIR signals (e.g. Godfrey-Smith *et al.*, 1988; Thomsen *et al.*, 2008; Murray *et al.*, 2012; Kars *et al.*, 2014b; Colarossi *et al.*, 2015; Möller and Murray, 2015; Sugisaki *et al.*, 2015). Based on this, Murray *et al.* (2012) suggested an approach to identify well-bleached quartz samples by comparing quartz and K-feldspar equivalent doses. Möller and Murray (2015) used this approach in a study of Swedish glaciofluvial samples and were able to conclude that the quartz OSL in about half of the samples was well bleached at deposition (based on agreement with IR_{50} and pIRIR signals). In our study, there is excellent agreement between the quartz OSL and K-feldspar $pIRIR_{290}$ ages for all the samples (Fig. 9[Q16]). Given the well-known difference in bleaching rates (see above), this similarity in ages suggests strongly that the quartz OSL signals in our samples must have been well bleached before final deposition (Fig. 9).

In addition, Buylaert *et al.* (2013) proposed an independent method to identify poorly bleached K-feldspar samples by comparing the IR_{50} to $pIRIR_{290}$ D_e ratios. Following a similar approach, we plotted the IR_{50} D_e value versus the corresponding $pIRIR_{290}$ equivalent dose for each sample (Fig. 8). First, it is interesting to note that the value of the intercept on the $pIRIR_{290}$ axis in Fig. 8 (i.e. 4.9 Gy) is indistinguishable from the difference between the values of 1.6 ± 0.3 and 5.9 ± 0.5 Gy inferred as IR_{50} and $pIRIR_{290}$ unbleachable residual doses, respectively, from the intercepts on the D_e axes in Fig. 7. Secondly, all data points lie on the same curve, indicating a good correlation of doses over a wide dose range (Fig. 8). Such smooth correlation implies that either all the samples were equally poorly bleached or they were well bleached. Given the heterogeneous nature of the bleaching process in space and time, the former seems unlikely. We conclude that these data suggest that both the feldspar signals from our samples were sufficiently bleached before deposition. Note that the poor dose recovery for the IR_{50} signals is most unlikely to perturb this conclusion. If poor dose recovery was to affect the conclusions drawn from this correlation, it would have to increase the scatter around the fitted line in Fig. 8; clearly, this cannot have happened to a significant degree. A similar conclusion was reached by Buylaert *et al.* (2013).

From the satisfactory dose recovery characteristics of the quartz OSL and K-feldspar $pIRIR_{290}$ signals and the excellent agreement between ages based on these signals, we conclude that the internal luminescence evidence suggests strongly that our quartz OSL ages are reliable and unlikely to have been significantly affected by incomplete bleaching. As the quartz signal is more readily reset, and there are potential complications in the $pIRIR_{290}$ ages arising from signal instability and residual dose subtraction, we use the quartz OSL ages in the next section.

OSL-CN age comparison

The quartz OSL ages are all concordant with the stratigraphy; they range from ~2 to 29 ka with the 11 (out of 13) OSL ages

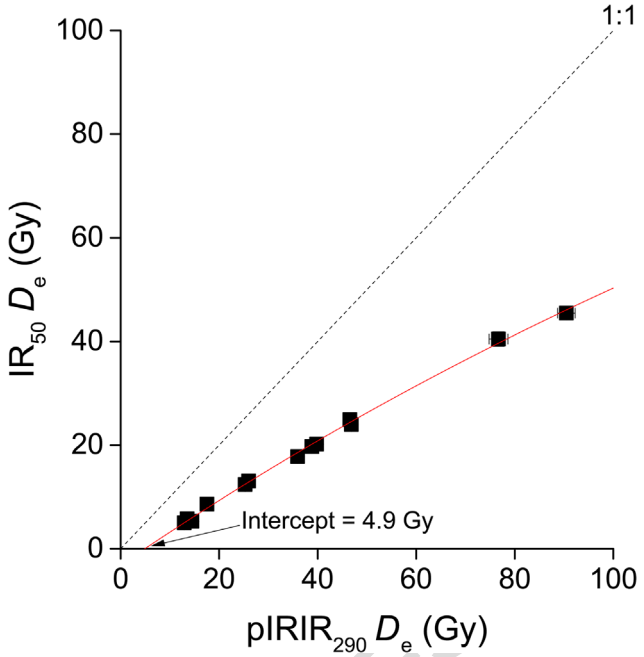

Figure 8. IR_{50} versus $pIRIR_{290}$ D_e values for all the samples. Each data point is an average of 12 aliquots. The error bars show one standard error. The solid line represents a saturating exponential function of the form $y = a(1-exp(-bx))$ fitted to the data. Q16

most closely related to the boulders consistently younger than ~13 ka. Figure 10 shows a schematic view of one of the boulders (PB2) together with the optical ages of the surrounding loess colluvium deposits as well as the ^{3}He surface-exposure age from the top of the boulder. It can be seen that the two samples collected below the boundary identified as the ground surface at the time of boulder emplacement have ages of 12.5 ± 1.1 ka (ROSL-05) and 12.0 ± 1.4 ka (ROSL-06), the weighted average of which provides a maximum age limit of 12.3 ± 1.0 ka for the boulder deposition. Furthermore, sample ROSL-04, taken from the colluvial wedge upslope of the boulder and thus deposited after the boulder, has an age

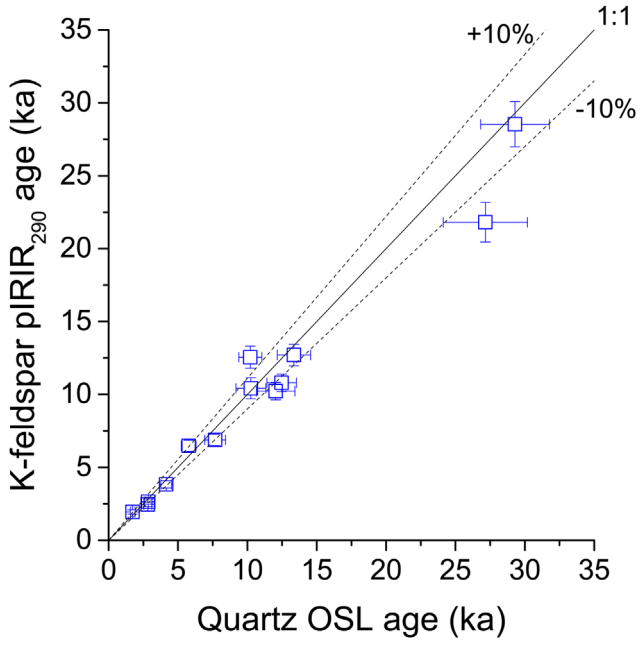

Figure 9. Comparison between quartz OSL and K-feldspar $pIRIR_{290}$ uncorrected ages. The dashed lines show 10% deviation from unity.

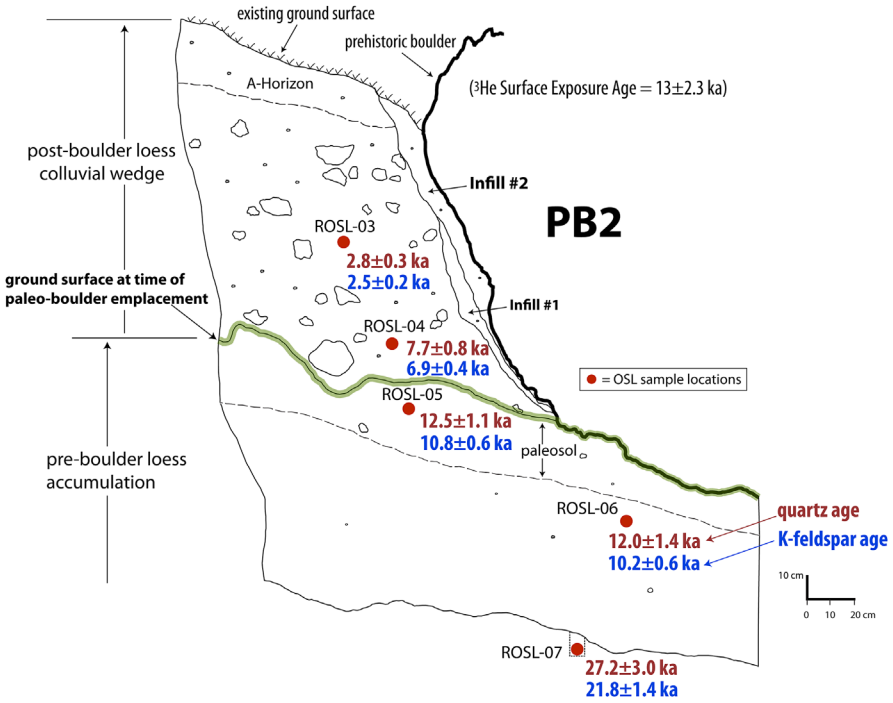

Figure 10. Schematic view of the same boulder as in Fig. 1(c) with the luminescence ages of the surrounding colluvium deposits as well as the ^{3}He exposure age of the surface of the boulder. Borella *et al.* (2016a, b).

of 7.7 ± 0.8 ka. These ages limit the boulder emplacement time to between 12.3 ± ~~1.0~~ and 7.7 ± 0.8 ka. The maximum age limit of 12.3 ± ~~1.0~~ ka is indistinguishable from the ^{3}He exposure age of 13 ± 2.3 ka from the top surface of the boulder. Our preferred interpretation is that (i) PB2 was emplaced at 12–14 ka (Mackey and Quigley, 2014), (ii) ^{3}He pre-detachment inheritance is negligible and (iii) the boulder emplacement time is indistinguishable from that of the underlying loess. In this instance, the possibility of significant ^{3}He inheritance is inconsistent with the optical chronology, highlighting the importance of these complementary data.

Maximum/minimum loess ages exist for only four of the boulders. Only one OSL sample (ROSL-02, 29 ± 2 ka) was taken in association with PB1 (from underneath) and there is no corresponding upslope sample to provide post-depositional age limit. Figure 11 summarizes the OSL age constraints and the ^{3}He surface-exposure age for the other four boulders (PB2, 3, 4, 5). The OSL ages associated with PB3 suggest an emplacement time between 2.9 ± 0.3 and 5.8 ± 0.5 ka, while the ^{3}He surface-exposure age from the top surface of the boulder is 8 ± 2 ka. Again the boulder age is indistinguishable from that of the underlying loess, suggesting that either boulder

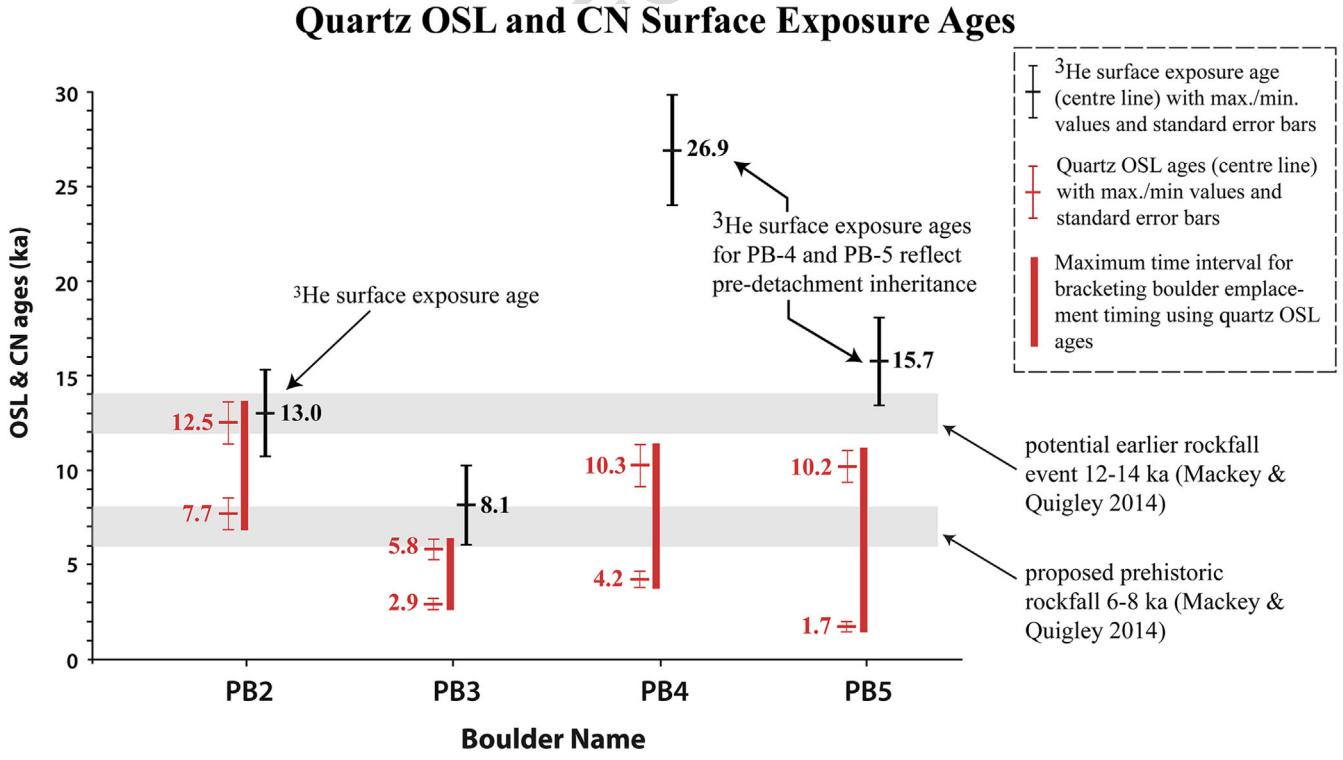

Figure 11. Quartz OSL age limits for the emplacement time of the boulders determined by dating loess deposits underlying boulders and loess–colluvium accumulated behind each boulder and the ^{3}He surface-exposure age from the surface of the boulder. From Borella *et al.* (2016a, b).

emplacement occurred at 5.8 ± 0.5 ka, or the boulder was emplaced after 5.8 ± 0.5 ka (and contained some ^{3}He inheritance) but before 2.9 ± 0.3 ka. In either case this boulder appears to have been emplaced significantly more recently than PB2 and is presumably associated with the 6–8 ka event (Mackey and Quigley, 2014).

In contrast, PB4 and PB5 have ^{3}He surface-exposure ages that are significantly older than the ages of the associated loess. PB4 has an exposure age of 26.9 ± 2.9 ka, while the OSL ages constrain the emplacement time to between 4.2 ± 0.4 and 10.2 ± 1.1 ka. Similarly, the OSL ages associated with PB5 suggest that it must have been deposited between 1.7 ± 0.2 and 10.2 ± 0.8 ka, whereas the ^{3}He age suggests an emplacement time of 15.7 ± 2.3 ka (Fig. 11). Given the internal stratigraphic consistency of the quartz OSL ages and their agreement both with K-feldspar ages and with the regional climate record (i.e. loess formation during the termination of LGM), we conclude that the discrepancy between the OSL and ^{3}He ages for PB4 and PB5 is most likely due to pre-detachment ^{3}He inheritance.

Conclusions

With respect to luminescence characteristics, the correlation between the IR_{50} and $pIRIR_{290}$ K-feldspar equivalent doses and the corresponding residual doses seems to provide a reliable method of determining the unbleachable residual dose present in these samples. Regardless of whether the IR_{50} equivalent doses are reliable or not (due to poor dose recovery), the comparison between the IR_{50} and pIRIR D_e values appears to provide a viable independent approach to identify well-bleached K-feldspar samples. The smooth correlation between the IR_{50} and $pIRIR_{290}$ D_e values over a wide dose range suggests strongly that all our samples were well bleached before final deposition on the slope. This is confirmed by the agreement between the quartz OSL and K-feldspar $pIRIR_{290}$ ages.

We successfully determined the emplacement time of palaeorockfall boulders by applying luminescence dating techniques to loess and colluvial (reworked) loess deposits in South Island, New Zealand. The quartz OSL and K-feldspar $pIRIR_{290}$ ages are all consistent with stratigraphy and in excellent agreement with each other for all the samples. To our knowledge, these are among the first reliable loess luminescence ages from New Zealand, although a few earlier studies have reported credible ages from non-loessic material.

Of the six loess samples immediately underlying the boulders the oldest has an age of ~13 ka, suggesting loess accumulation or subsequent sediment reworking/remobilization within the upper section of the loess (i.e. soil horizon) after termination of the LGM and implying that any prehistoric rockfall boulder emplaced before ~13 ka is unlikely to be observable at the surface due to burial (Mackey and Quigley, 2014). The emplacement time of individual boulders is further constrained by luminescence dating of colluvial (reworked) loess deposits upslope of individual boulders. Overall, the optical ages are consistent with both a prehistoric rockfall event at 6–8 ka and a possible preceding event at 12–14 ka (Mackey and Quigley, 2014), although the temporal resolution of boulders' emplacement time is 3–9 ka. This resolution is not limited by age uncertainties but rather by the stratigraphy; there was simply no material deposited closer to the time of emplacement.

If we take the optical ages at face values, three boulders can only be associated with the 6–8 ka event and one with the 12–14 ka event. Furthermore, a comparison of luminescence ages with ^{3}He surface-exposure ages from the surfaces of each boulder enables us to identify two boulders containing significant cosmogenic ^{3}He inheritance and two for which any inheritance is probably negligible or small, demonstrating the great advantage of a multi-technique approach in geochronology.

Acknowledgements. R.S. would like to thank Carlsberg Foundation for financial support (Grant No. 2012_01 _0838) during this project. Joy Mailand-Hansen is thanked for sample preparation. The New Zealand Earthquake Commission is acknowledged for provision of finances under a Capability Grant and a PhD scholarship to J.B. Frontiers Abroad also provided financial support for this research. J.P. B. thanks the Danish Council for Independent Research – Matural Sciences (FNU) for financial support (Steno Grant No. 11-104566). We would also like to thank Dr Peter Almond and an anonymous reviewer for their constructive comments on the manuscript.

Supplementary material

Table S1 Outline of the quartz OSL (Murray and Wintle, 2003) and K-feldspar $pIRIR_{290}$ (Thiel *et al.*, 2011) SAR protocols.

Abbreviations. CN, cosmogenic nuclide; IR, infrared; IRSL, infrared stimulated luminescence; LGM, Last Glacial Maximum; OSL, optically stimulated luminescence; pIRIR, post-IR IRSL; SAR, single-aliquot regenerative-dose; TL, thermoluminescence.

References

Aitken MJ. 1985. *Thermoluminescence Dating*. Academic Press: London.

Aitken MJ. 1998. *An Introduction to Optical Dating: the Dating of Quaternary Sediments by the Use of Photon-Stimulated Luminescence*. Oxford University Press: Oxford.

Almond PC, Moar NT, Lian OB. 2001. Reinterpretation of the glacial chronology of South Westland, New Zealand. *New Zealand Journal of Geology and Geophysics* **44**: 1–15.

Almond PC, Shanhun FL, Rieser U *et al.* 2007. An OSL, radiocarbon and tephra isochron-based chronology for Birdlings Flat loess at Ahuriri Quarry, Banks Peninsula, Canterbury, New Zealand. *Quaternary Geochronology* **2**: 4–8.

André M. 1997. Holocene rockwall retreat in Svalbard: a triple-rate evolution. *Earth Surface Processes and Landforms* **22**: 423–440.

Auclair M, Lamothe M, Huot S. 2003. Measurement of anomalous fading for feldspar IRSL using SAR. *Radiation Measurements* **37**: 487–492.

Baillifard F, Jaboyedoff M, Sartori M. 2003. Rockfall hazard mapping along a mountainous road in Switzerland using a GIS-based parameter rating approach. *Natural Hazards and Earth System Science* **3**: 435–442.

Balescu S, Ritz J, Lamothe M *et al.* 2007. Luminescence dating of a gigantic palaeolandslide in the Gobi-Altay mountains, Mongolia. *Quaternary Geochronology* **2**: 290–295.

Berger G, Pillans BJ, Bruce JG *et al.* 2002. Luminescence chronology of loess-paleosol sequences from southern South Island, New Zealand. *Quaternary Science Reviews* **21**: 1899–1913.

Berger GW, Almond PC, Pillans BJ. 2001a. Luminescence dating and glacial stratigraphy in Westland, New Zealand. *New Zealand Journal of Geology and Geophysics* **44**: 25–35.

Berger GW, Pillans BJ, Tonkin PJ. 2001b. Luminescence chronology of loess-paleosol sequences from Canterbury, South Island, New Zealand. *New Zealand Journal of Geology and Geophysics* **44**: 501–516.

Bertolini G. 2007.[Q17] Radiocarbon dating on landslides in the Northern Apennines (Italy). In *Landslides and Climate Changes*, McInnes, Jakeways, Fairbank, Mathie (eds). Taylor & Francis: London; 73–80. Q17

Borella J, Quigley M, Sohbati R *et al.* 2016a. Stratigraphy and chronology of late Quaternary loessic hillslope sediments reveals seismic, climatic, and anthropogenic influences on surface processes,

eastern South Island, New Zealand. *Journal of Quaternary Science* (in press).
Borella J, Quigley M, Vick L. 2016b. Anthropocene rockfalls travel farther than prehistoric predecessors. *Science Advances* ~~(in press)~~.
Budetta P. 2004. Assessment of rockfall risk along roads. *Natural Hazards and Earth System Science* **4**: 71–81.
Bull WB, King J, Kong F *et al.* 1994. Lichen dating of coseismic landslide hazards in alpine mountains. *Geomorphology* **10**: 253–264.
Bunce CM, Cruden DM, Morgenstern NR. 1997. Assessment[Q18] of the hazard from rock fall on a highway. *Canadian Geotechnical Journal* **34**: 344–356.
Buylaert J, Jain M, Murray AS *et al.* 2012. A robust feldspar luminescence dating method for Middle and Late Pleistocene sediments. *Boreas* **41**: 435–451.
Buylaert J, Thiel C, Murray A, *et al.* 2011. IRSL and post-IR IRSL residual doses recorded in modern dust samples from the Chinese Loess Plateau. *Geochronometria* **38**: 432–440.
Buylaert J.-P, Murray AS, Gebhardt AC *et al.* 2013. Luminescence dating of the PASADO core 5022-1D from Laguna Potrok Aike (Argentina) using IRSL signals from feldspar. *Quaternary Science Reviews* **71**: 70–80.
Buylaert J.-P, Murray AS, Thomsen KJ *et al.* 2009. Testing the potential of an elevated temperature IRSL signal from K-feldspar. *Radiation Measurements* **44**: 560–565.
Chapot MS, Sohbati R, Murray AS *et al.* 2012. Constraining the age of rock art by dating a rockfall event using sediment and rock-surface luminescence dating techniques. *Quaternary Geochronology* **13**: 18–25.
Colarossi D, Duller GAT, Roberts HM *et al.* 2015. Comparison of paired quartz OSL and feldspar post-IR IRSL dose distributions in poorly bleached fluvial sediments from South Africa. *Quaternary Geochronology* **30**: 233–238.
Cunningham AC, Wallinga J. 2010. Selection of integration time intervals for quartz OSL decay curves. *Quaternary Geochronology* **5**: 657–666.
Dilley M, Chen RS, Deichmann U, *et al.* 2005. Natural disaster hotspots: a global risk analysis. In *Disaster Risk Management Series*. The World Bank: Washington, DC; Issue No. 5. Evans SG, Hungr O. 1993. The assessment of rockfall hazard at the base of talus slopes. *Canadian Geotechnical Journal* **30**: 620–636.
Fuchs M, Lang A. 2009. Luminescence dating of hillslope deposits – a review. *Geomorphology* **109**: 17–26.
Godfrey-Smith DI, Huntley DJ, Chen W. 1988. Optical dating studies of quartz and feldspar sediment extracts. *Quaternary Science Reviews* **7**: 373–380.
Guérin G, Mercier N, Adamiec G. 2011. Dose-rate conversion factors: update. *Ancient TL* **29**: 5–8.
Guzzetti F. 2000. Landslide fatalities and the evaluation of landslide risk in Italy. *Engineering Geology* **58**: 89–107.
Heron D, Lukovic B, Massey C *et al.* 2014. GIS modelling in support of earthquake-induced rockfall and cliff collapse risk assessment in the Port Hills, Christchurch. *Journal of Spatial Science* **59**: 313–332.
Holdaway RN, Roberts RG, Beavan-Athfield NR *et al.* 2002. Optical dating of quartz sediments and accelerator mass spectrometry ^{14}C dating of bone gelatin and moa eggshell: a comparison of age estimates for non-archaeological deposits in New Zealand. *Journal of the Royal Society of New Zealand* **32**: 463–505.
Hornblow S, Quigley M, Nicol A *et al.* 2014. Paleoseismology of the 2010 Mw 7.1 Darfield (Canterbury) earthquake source, Greendale Fault, New Zealand. *Tectonophysics* **637**: 178–190.
Hungr O, Evans SG, Hazzard J. 1999. Magnitude and frequency of rock falls and rock slides along the main transportation corridors of southwestern British Columbia. *Canadian Geotechnical Journal* **36**: 224–238.
Huntley D, Baril M. 1997. The K content of the K-feldspars being measured in optical dating or in thermoluminescence dating. *Ancient TL* **15**: 11–13.
Huntley DJ, Hancock RGV. 2001. The Rb contents of the K-feldspar grains being measured in optical dating. *Ancient TL* **19**: 43–46.
Huntley DJ, Lamothe M. 2001. Ubiquity of anomalous fading in K-feldspars and the measurement and correction for it in optical dating. *Canadian Journal of Earth Sciences* **38**: 1093–1106.
Jain M, Murray AS, Bøtter-Jensen L. 2003. Characterisation of blue-light stimulated luminescence components in different quartz samples: implications for dose measurement. *Radiation Measurements* **37**: 441–449.
Jain M, Sohbati R, Guralnik B *et al.* 2015. Kinetics of infrared stimulated luminescence from feldspars. *Radiation Measurements* **81**: 242–250. Q18
Kars RH, Reimann T, Ankjaergaard C *et al.* 2014b. Bleaching of the post-IR IRSL signal: new insights for feldspar luminescence dating. *Boreas* **43**: 780–791.
Kars RH, Reimann T, Wallinga J. 2014a. Are feldspar SAR protocols appropriate for post-IR IRSL dating? *Quaternary Geochronology* **22**: 126–136.
Keefer DK. 1984. Landslides caused by earthquakes. *Geological Society of America Bulletin* **95**: 406–421.
Lang A, Moya J, Corominas J *et al.* 1999. Classic and new dating methods for assessing the temporal occurrence of mass movements. *Geomorphology* **30**: 33–52.
Li B, Li S. 2006. Comparison of estimates using the fast component and the medium component of quartz OSL. *Radiation Measurements* **41**: 125–136.
Li B, Roberts RG, Jacobs Z. 2013. On the dose dependency of the bleachable and non-bleachable components of IRSL from K-feldspar: improved procedures for luminescence dating of Quaternary sediments. *Quaternary Geochronology* **17**: 1–13.
Li G, Wen L, Xia D *et al.* 2015. Quartz OSL and K-feldspar pIRIR dating of a loess/paleosol sequence from arid central Asia, Tianshan Mountains, NW China. *Quaternary Geochronology* **28**: 40–53.[Q19] Q19
Litchfield NJ, Lian OB. 2004. Luminescence age estimates of Pleistocene marine terrace and alluvial fan sediments associated with tectonic activity along coastal Otago, New Zealand. *New Zealand Journal of Geology, and Geophysics* **47**: 29–37.
Lowick SE, Trauerstein M, Preusser F. 2012. Testing the application of post IR-IRSL dating to fine grain waterlain sediments. *Quaternary Geochronology* **8**: 33–40.
Luckman BH, Fiske CJ. 1995. Estimating long-term rockfall accretion rates by lichenometry. In *Steepland Geomorphology*, Slaymaker O (ed.). Wiley: Chichester; 233–255.
Mackey BH, Quigley MC. 2014. Strong proximal earthquakes revealed by cosmogenic ^{3}He dating of prehistoric rockfalls, Christchurch, New Zealand. *Geology* **42**: 975–978.
Massey CI, McSaveney MJ, Taig T *et al.* 2014. Determining rockfall risk in Christchurch using rockfalls triggered by the 2010–2011 Canterbury earthquake sequence. *Earthquake Spectra* **30**: 155–181.
Matmon A, Shaked Y, Porat N *et al.* 2005. Landscape development in an hyperarid sandstone environment along the margins of the Dead Sea fault: implications from dated rock falls. *Earth and Planetary Science Letters* **240**: 803–817.
McCarroll D, Shakesby RA, Matthews JA. 2001. Enhanced rockfall activity during the little ice age: further lichenometric evidence from a Norwegian talus. *Permafrost and Periglacial Processes* **12**: 157–164.
Mejdahl V. 1987. Internal radioactivity in quartz and feldspar grains. *Ancient TL*.[Q20] Q20
Möller P, Murray AS. 2015. Drumlinised glaciofluvial and glaciolacustrine sediments on the Småland peneplain, South Sweden – new information on the growth and decay history of the Fennoscandian Ice Sheets during MIS 3. *Quaternary Science Reviews* **122**: 1–29.
Murray AS, Schmidt ED, Stevens T *et al.* 2014. Dating Middle Pleistocene loess from stari slankamen (Vojvodina, Serbia) – limitations imposed by the saturation behaviour of an elevated temperature IRSL signal. *Catena* **117**: 34–42.
Murray AS, Thomsen KJ, Masuda N *et al.* 2012. Identifying well-bleached quartz using the different bleaching rates of quartz and feldspar luminescence signals. *Radiation Measurements* **47**: 688–695.

Murray AS, Wintle AG. 2000. Luminescence dating of quartz using an improved single-aliquot regenerative-dose protocol. *Radiation Measurements* **32**: 57–73.

Murray AS, Wintle AG. 2003. The single aliquot regenerative dose protocol: potential for improvements in reliability. *Radiation Measurements* **37**: 377–381.

Nesje A, Blikra LH, Anda E. 1994. Dating rockfall-avalanche deposits from degree of rock-surface weathering by Schmidt-hammer tests: a study from Norangsdalen, Sunnmøre, Norway. Q21

Panek T. 2015. Recent progress in landslide dating: a global overview. *Progress in Physical Geography* **39**: 168–198.

Preusser F, Andersen BG, Denton GH *et al.* 2005. Luminescence chronology of Late Pleistocene glacial deposits in North Westland, New Zealand. *Quaternary Science Reviews* **24**: 2207–2227.

Preusser F, Ramseyer K, Schlüchter C. 2006. Characterisation of low OSL intensity quartz from the New Zealand Alps. *Radiation Measurements* **41**: 871–877.

Reimann T, Tsukamoto S. 2012. Dating the recent past (<500 years) by post-IR IRSL feldspar – examples from the North Sea and Baltic Sea coast. *Quaternary Geochronology* **10**: 180–187.

Rinat Y, Matmon A, Arnold M *et al.* 2014. Holocene rockfalls in the southern Negev Desert, Israel and their relation to Dead Sea fault earthquakes. *Quaternary Research* **81**: 260–273.

Roberts HM. 2012. Testing post-IR IRSL protocols for minimising fading in feldspars, using Alaskan loess with independent chronological control. *Radiation Measurements* **47**: 716–724.

Roskosch J, Tsukamoto S, Meinsen J *et al.* 2012. Luminescence dating of an Upper Pleistocene alluvial fan and aeolian sandsheet complex: the Senne in the Münsterland Embayment, NW Germany. *Quaternary Geochronology* **10**: 94–101.

Schatz A, Buylaert J, Murray A *et al.* 2012. Establishing a luminescence chronology for a palaeosol-loess profile at Tokaj (Hungary): A comparison of quartz OSL and polymineral IRSL signals. *Quaternary Geochronology* **10**: 68–74.

Sohbati R, Murray A, Jain M *et al.* 2013. Na-rich feldspar as a luminescence dosimeter in infrared stimulated luminescence (IRSL) dating. *Radiation Measurements* **51–52**: 67–82.

Sohbati R, Murray AS, Buylaert J *et al.* 2012. Luminescence dating of Pleistocene alluvial sediments affected by the Alhama de Murcia fault (eastern Betics, Spain) – a comparison between OSL, IRSL and post-IRIRSL ages. *Boreas* **41**: 250–262.

Spooner NA. 1994. The anomalous fading of infrared-stimulated luminescence from feldspars. *Radiation Measurements* **23**: 625–632.

Stevens T, Marković SB, Zech M *et al.* 2011. Dust deposition and climate in the Carpathian Basin over an independently dated last glacial–interglacial cycle. *Quaternary Science Reviews* **30**: 662–681.

Stock GM, Collins BD. 2014. Reducing rockfall risk in Yosemite National Park. *Eos, Transactions American Geophysical Union* **95**: 261–263.

Stoffel M. 2006. A review of studies dealing with tree rings and rockfall activity: the role of dendrogeomorphology in natural hazard research. *Natural Hazards* **39**: 51–70.

Stout ML. 1969. Radiocarbon dating of landslides in southern California and engineering geology implications. *Geological Society of America Special Papers* **123**: 167–180.

Sugisaki S, Buylaert J, Murray A *et al.* 2015. OSL dating of fine-grained quartz from Holocene Yangtze Delta sediments. *Quaternary Geochronology* **30**: 226–232.

Talebian M, Fielding EJ, Funning GJ, *et al.* 2004. The 2003 Bam (Iran) earthquake: rupture of a blind strike-slip fault. *Geophysical Research Letters* **31**: 2–5. Q21

Thiel C, Buylaert J, Murray A *et al.* 2011. Luminescence dating of the Stratzing loess profile (Austria) – testing the potential of an elevated temperature post-IR IRSL protocol. *Quaternary International* **234**: 23–31.

Thomsen KJ, Murray AS, Jain M *et al.* 2008. Laboratory fading rates of various luminescence signals from feldspar-rich sediment extracts. *Radiation Measurements* **43**: 1474–1486.

Tsukamoto S, Kataoka K, Miyabuchi Y. 2013. Luminescence dating of volcanogenic outburst flood sediments from Aso volcano and tephric loess deposits, southwest Japan. *Geochronometria* **40**: 294–303.

Vandenberghe D, De Corte F, Buylaert J.-P *et al.* 2008. On the internal radioactivity in quartz. *Radiation Measurements* **43**: 771–775.

Vandergoes MJ, Hogg AG, Lowe DJ *et al.* 2013. A revised age for the Kawakawa/Oruanui tephra, a key marker for the Last Glacial Maximum in New Zealand. *Quaternary Science Reviews* **74**: 195–201.

Veit H, Preusser F, Trauerstein M. 2015. The southern westerlies in Central Chile during the two last glacial cycles as documented by coastal aeolian sand deposits and intercalating palaeosols. *Catena* **134**: 30–40.

Villaseñor T, Jaeger JM, Foster DA. 2016. Linking Late Pleistocene alpine glacial erosion and continental margin sedimentation: insights from $^{40}Ar/^{39}Ar$ dating of silt-sized sediment, Canterbury Basin, New Zealand. *Earth and Planetary Science Letters* **433**: 303–316.

Wallinga J, Bos AJJ, Dorenbos P *et al.* 2007. A test case for anomalous fading correction in IRSL dating. *Quaternary Geochronology* **2**: 216–221.

Wallinga J, Murray A, Duller G. 2000. Underestimation of equivalent dose in single-aliquot optical dating of feldspars caused by preheating. *Radiation Measurements* **32**: 691–695.

Wintle AG. 1973. Anomalous fading of thermo-luminescence in mineral samples. *Nature* **245**: 143–144. Q22

Yi S, Buylaert J.-P, Murray AS *et al.* 2015. High resolution OSL and post-IR IRSL dating of the last interglacial–glacial cycle at the Sanbahuo loess site (northeastern China). *Quaternary Geochronology* **30B**: 200–206.

Yin Y, Wang F, Sun P. 2009. Landslide hazards triggered by the 2008 Wenchuan earthquake, Sichuan, China. *Landslides* **6**: 139–152.